Обзор ArXiv: astro-ph, 7-10 February 2017

От Сильченко О.К.

Astro-ph: 1702.02118

The JCMT Nearby Galaxies Legacy Survey – XI. – Environmental Variations in the Atomic and Molecular Gas Radial Profiles of Nearby Spiral Galaxies

Angus Mok [1], C. D. Wilson[1], J. H. Knapen[2,3], J. R. Sánchez-Gallego[4], E. Brinks[5], and E. Rosolowsky[6]

[1] *Department of Physics & Astronomy, McMaster University, Hamilton, Ontario L8S 4M1, Canada*
[2] *Instituto de Astrofísica de Canarias, E-38205 La Laguna, Tenerife, Spain*
[3] *Departamento de Astrofísica, Universidad de La Laguna, E-38200 La Laguna, Tenerife, Spain*
[4] *Department of Physics and Astronomy, University of Kentucky, 40506-0055, Lexington, Kentucky, United States*
[5] *Centre for Astrophysics Research, University of Hertfordshire, AL10 9AB, Hatfield, Hertfordshire, United Kingdom*
[6] *Department of Physics, University of Alberta, Edmonton, Ontario T6G 2R3, Canada*

8 February 2017

ABSTRACT

We present an analysis of the radial profiles of a sample of 43 H I -flux selected spiral galaxies from the Nearby Galaxies Legacy Survey (NGLS) with resolved James Clerk Maxwell Telescope (JCMT) CO $J = 3-2$ and/or Very Large Array (VLA) H I maps. Comparing the Virgo and non-Virgo populations, we confirm that the H I disks are truncated in the Virgo sample,

Выборка; выделены галактики, имеющие ВСЕ данные

Galaxy[1]	Env[2]	H I source	H I beam size[3]	H I rms[3]	H_2[4]	Hα	Incl	Dist
-	-	-	-	[mJy/beam]	-	-	[deg]	[Mpc]
NGC0210	F	15B-111	66"×46"	1.75	D	HRS	55.4	22.4
NGC3437	F	-	-	-	D	HRS	72.8	20.1
NGC6140	F	AW701	60"×45"	2.16	ND	NGLS	32.2	17.8
NGC7742	F	15B-111	51"×49"	1.57	D	HRS	16.8	24.8
IC0750	G	AW701	51"×49"	1.30	D	NGLS	65.8	8.3
IC3908	G	-	-	-	D	HRS	73.2	19.0
NGC0450	G	-	-	-	D	NGLS	49.8	25.4
NGC1140	G	15B-111	79"×44"	1.51	ND	NGLS	73.8	20.1
NGC1325	G	15B-111	66"×47"	1.74	ND	NGLS	74.3	20.7
NGC2146A	G	AW701	63"×46"	1.50	ND	NGLS	69	25.9
NGC2742	G	AW701	62"×45"	1.24	D	NGLS	60.6	22.4
NGC3077	G	THINGS	14"×13"	0.94	D	NGLS	38.1	3.9
NGC3162	G	-	-	-	D	NGLS	37.1	20.7
NGC3227	G	-	-	-	D	NGLS	68.3	18.4
NGC3346	G	-	-	-	D	HRS	34.1	19.5
NGC3507	G	-	-	-	D	NGLS	31.9	15.5
NGC3684	G	-	-	-	D	HRS	50.8	18.4
NGC3782	G	AW701	51"×49"	1.26	ND	NGLS	60.3	14.3
NGC3982	G	-	-	-	D	HRS	29.9	20.1
NGC4041	G	-	-	-	D	NGLS	22	21.9
NGC4123	G	-	-	-	D	HRS	44.3	20.1
NGC4713	G	VIVA	26"×22"	1.96	D	HRS	23.8	10.9
NGC4771	G	-	-	-	D	HRS	74.4	17.2
NGC4772	G	VIVA	18"×15"	0.36	ND	NGLS	67.3	16.1
NGC4775	G	-	-	-	D	HRS	28.4	23.0
NGC4808	G	VIVA	40"×36"	0.59	D	HRS	69.2	12.0
NGC4254	V	VIVA	38"×33"	0.41	D	NGLS	20.1	16.7
NGC4273	V	-	-	-	D	GOLDMINE	26.9	16.7
NGC4294	V	VIVA	29"×27"	0.29	ND	HRS	70.2	16.7
NGC4298	V	VIVA	17"×16"	0.35	D	NGLS	58.4	16.7
NGC4303	V	-	-	-	D	HRS	18.1	16.7
NGC4383	V	VIVA	45"×38"	0.26	D	NGLS	63.7	16.7
NGC4390	V	AW701	58"×53"	1.16	ND	NGLS	43.3	16.7
NGC4396	V	VIVA	27"×27"	0.28	ND	HRS	71.6	16.7
NGC4430	V	-	-	-	D	NGLS	43.8	16.7
NGC4480	V	-	-	-	D	HRS	61.2	16.7
NGC4548	V	VIVA	17"×16"	0.30	ND	HRS	36.9	16.7
NGC4567	V	VIVA	17"×16"	0.36	D	NGLS	39.4	16.7
NGC4568	V	VIVA	17"×16"	0.36	D	NGLS	67.5	16.7
NGC4579	V	VIVA	42"×35"	0.45	D	NGLS	41.9	16.7
NGC4647	V	-	-	-	D	NGLS	31.6	16.7
NGC4651	V	VIVA	17"×16"	0.40	D	NGLS	49.5	16.7
NGC4654	V	VIVA	16"×16"	0.45	D	HRS	59.8	16.7

Сравнение выборок в скоплении и в поле+группы

Table 2. Global Properties of the non-Virgo and Virgo Resolved Samples

Mean Quantity	Non-Virgo (26)	Virgo (17)	KS - Test
$\log M_{H_I}$ [$M_\odot$]	9.24 ± 0.05	9.04 ± 0.08	$\underline{0.009}$
$\log M_*$ [$M_\odot$]	9.87 ± 0.07	10.05 ± 0.12	0.154
M_{H_I}/M_*	0.35 ± 0.06	0.15 ± 0.03	0.108
Distance [kpc]	18.6 ± 0.94	16.0	-
$\log$ SFR [$M_\odot$ yr^{-1}]	-0.29 ± 0.09	-0.25 ± 0.14	0.774
$\log$ sSFR [yr^{-1}]	-10.17 ± 0.09	-10.30 ± 0.10	0.610
$\log M_{H_I}$/SFR [yr]	9.54 ± 0.07	9.29 ± 0.11	0.486
$\log M_{H_2}$ [1] [$M_\odot$]	8.35 ± 0.11	8.83 ± 0.13	$\underline{0.028}$ [2]
$\log$ SFR/M_{H_2} [1] [yr]	-8.62 ± 0.11	-9.06 ± 0.10	$\underline{0.049}$ [2]
M_{H_2}/M_* [1]	0.047 ± 0.012	0.095 ± 0.016	0.051 [2]
M_{H_2}/M_{H_I} [1]	0.38 ± 0.14	1.43 ± 0.37	$\underline{0.007}$ [2]
$M_{H_2} + M_{H_I}$ [$M_\odot$] [1]	9.35 ± 0.05	9.35 ± 0.10	0.656 [2]

Note: Underline indicates $p < 0.05$.
[1] CO non-detections taken into account using survival analysis; please refer to Mok et al. (2016) for more information.
[2] Log-rank test used, which takes into account censored data.

Профили HI

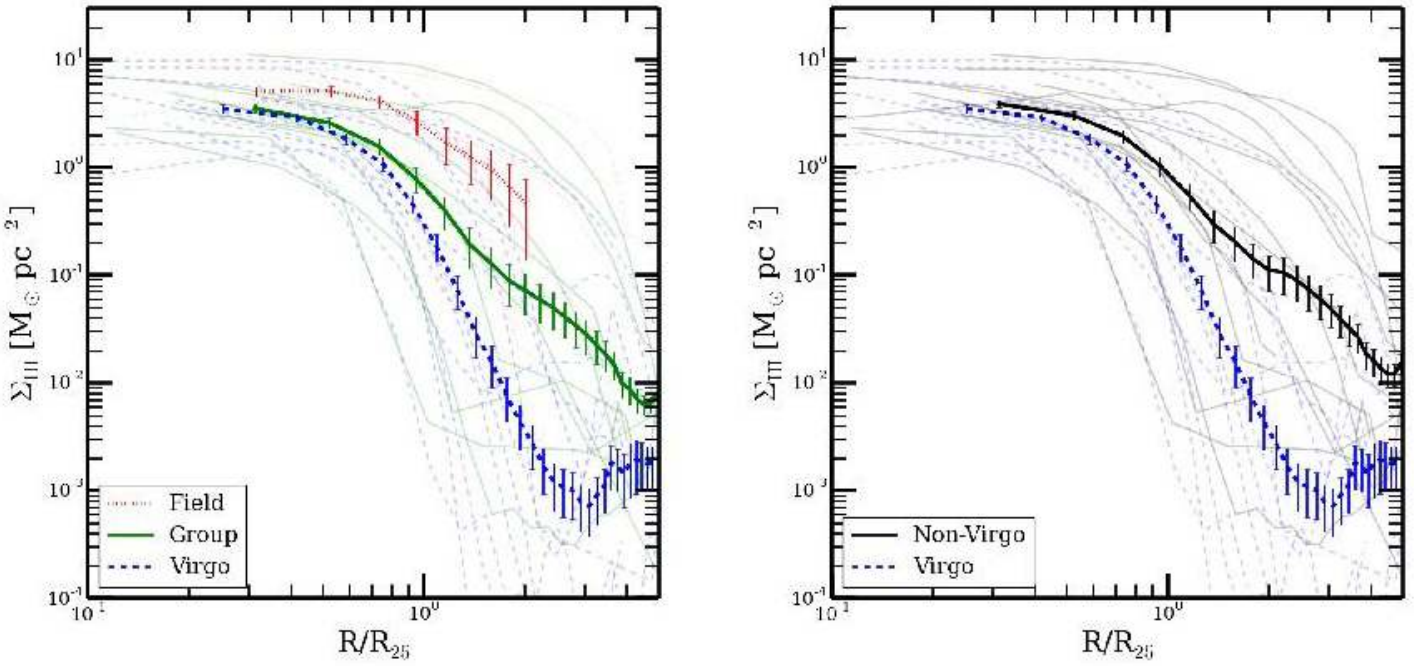

Figure 3. The radial profiles of H I surface density for the galaxies in our sample, calculated using the geometric mean method and normalized by R_{25}. The statistical error bars for each profile are plotted. The individual galaxy profiles are in the background. **Left:** The sample is separated into field (red-dotted), group (green), and Virgo (blue-dashed) populations. We see a reduction in the sizes of the H I disk, from field to group to the Virgo Cluster, suggesting H I properties are affected even in moderate density environments. **Right:** The sample is separated into the non-Virgo (black) and Virgo (blue-dashed) populations. Even for this H I-flux selected sample, the Virgo Cluster galaxies have truncated H I distributions in the outskirts compared to non-Virgo galaxies.

Профили молекулярного газа и темпов звездообразования

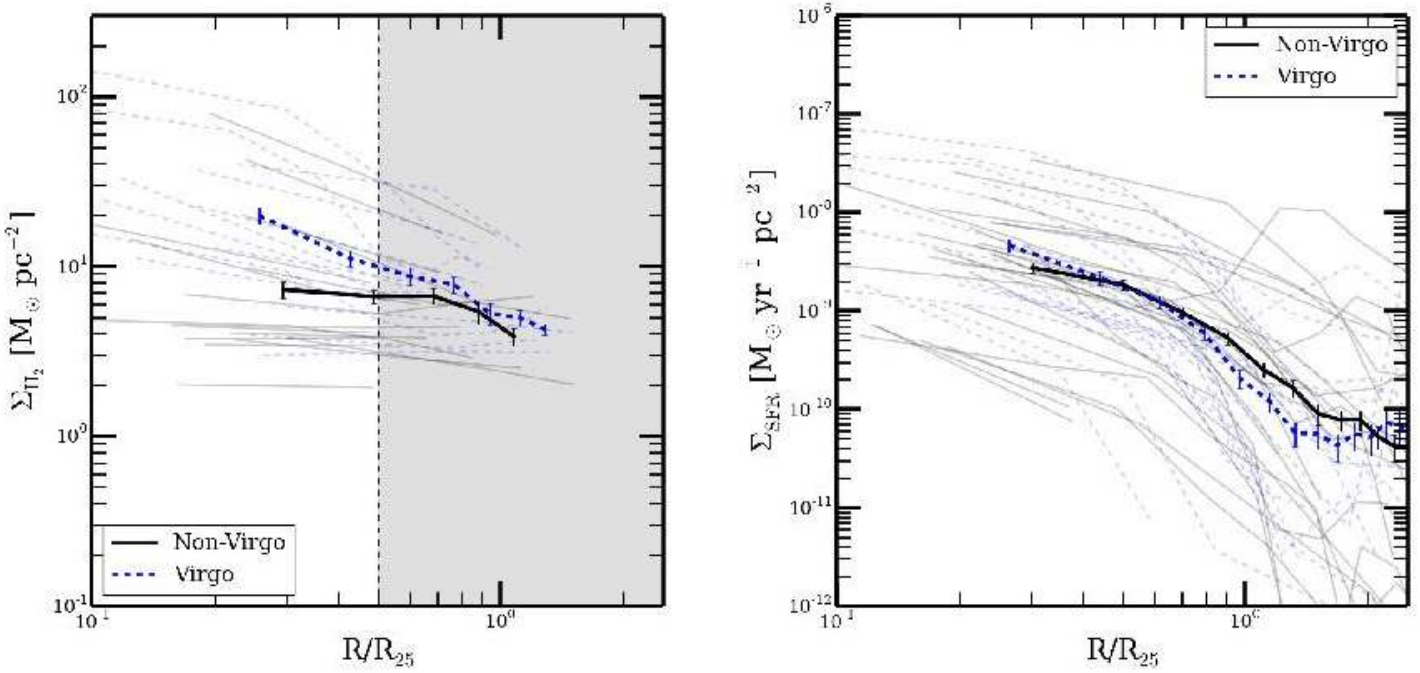

Figure 4. Left: The radial profiles of H_2 surface density for the galaxies in our sample, calculated using the geometric mean method and normalized by R_{25}. The statistical error bars for each profile are plotted. The individual galaxy profiles are in the background. The sample is separated into the non-Virgo (black) and Virgo (blue-dashed) populations. The dashed vertical line is at $R_{25} = 0.5$, the main target area of the NGLS survey, and results from the CO $J = 3 - 2$ maps are less reliable in the shaded region. On average, the Virgo galaxies are more H_2-rich at all radii, along with a steeper radial gradient. **Right:** The radial profiles of star formation rate surface density for the galaxies in our sample, calculated using the geometric mean method and normalized by R_{25}. The statistical error bars for each profile are plotted. The individual galaxy profiles are in the background. We see an enhancement in the star formation rates near the centre of Virgo galaxies, similar to the behaviour of the H_2 distribution. However, there are also hints of a truncation in their disks at large radii.

Еще сравнение Virgo- неVirgo

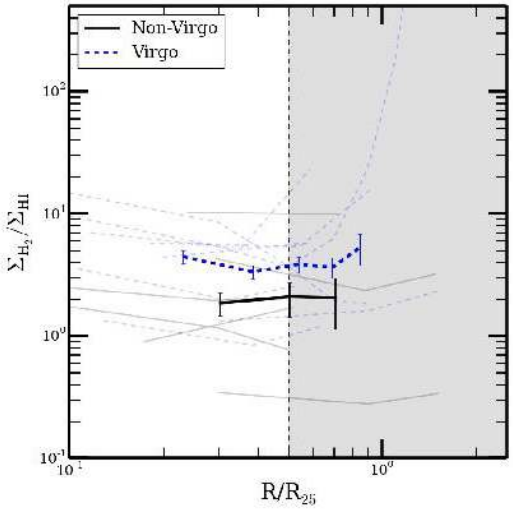

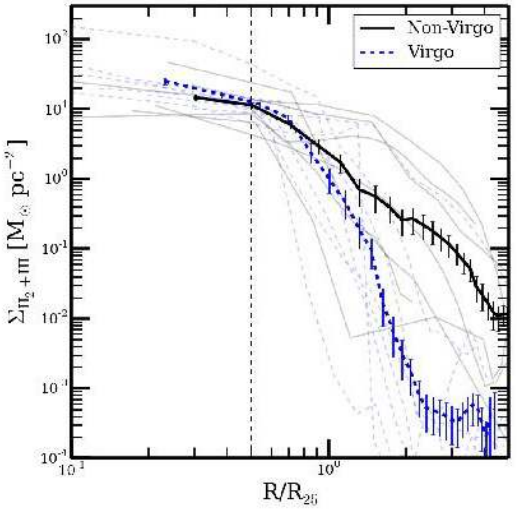

Figure 5. Left: The mean radial profiles of the H_2-to-H I ratio for the galaxies in our sample, calculated using the geometric mean method an by R_{25}. The statistical error bars for each profile are plotted. The individual galaxy profiles are in the background. The sample is separated into t (black) and Virgo (blue-dashed) populations. The dashed vertical line is at $R_{25} = 0.5$, the main target area of the NGLS survey, and results $J = 3 - 2$ maps are less reliable in the shaded region. The H_2-to-H I ratio shows an enhancement for Virgo galaxies, especially near the c The radial profiles of the total gas surface density for the galaxies in our sample, calculated using the geometric mean method and normalized statistical error bars for each profile are plotted. The individual galaxy profiles are in the background. There is a steeper radial distribution for V compared to non-Virgo galaxies, with more gas concentrated near the centre. Ram pressure stripping is likely playing a role in removing low d the outskirts and enhancing the high density gas near the centre.

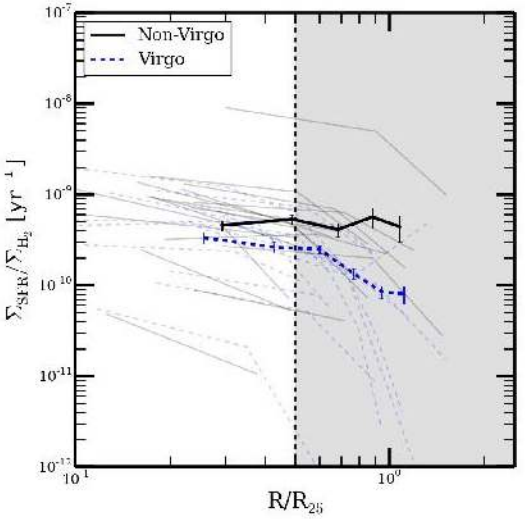

Figure 6. The SFR/H_2 surface density radial profiles for the galaxies in our sample, calculated using the geometric mean method and normalized by R_{25}. The statistical error bars for each profile are plotted. The individual galaxy profiles are in the background. The sample is separated into the non-Virgo (black) and Virgo (blue-dashed) populations. The dashed vertical line is at $R_{25} = 0.5$, the main target area of the NGLS survey, and results from the CO $J = 3 - 2$ maps are less reliable in the shaded region. Both profiles show a relatively flat trend with radius, with the Virgo galaxies offset at a lower star formation efficiency (or longer molecular gas depletion time),

Astro-ph: 1702.02392

CONNECTION BETWEEN STELLAR MASS DISTRIBUTIONS WITHIN GALAXIES AND QUENCHING SINCE $Z = 2$

MOEIN MOSLEH [1,2], SANDRO TACCHELLA [3], ALVIO RENZINI [4], C. MARCELLA CAROLLO [3], ALIREZA MOLAEINEZHAD [1], MASATO ONODERA [5], HABIB G. KHOSROSHAHI [1], SIMON LILLY [3]

Accepted for publication in ApJ

Abstract

We study the history from $z \sim 2$ to $z \sim 0$ of the stellar mass assembly of quiescent and star-forming galaxies in a spatially resolved fashion. For this purpose we use multi-wavelength imaging data from the Hubble Space Telescope (HST) over the GOODS fields and the Sloan Digital Sky Survey (SDSS) for the local population. We present the radial stellar mass surface density profiles of galaxies with $M_* > 10^{10} M_\odot$, corrected for mass-to-light ratio (M_*/L) variations, and derive the half-mass radius (R_m), central stellar mass surface density within 1 kpc (Σ_1) and surface density at R_m (Σ_m) for star-forming and quiescent galaxies and study their evolution with redshift. At fixed stellar mass, the *half-mass sizes* of quiescent galaxies increase from $z \sim 2$ to $z \sim 0$ by a factor of $\sim 3-5$, whereas the half-mass sizes of star-forming galaxies increase only slightly, by a factor of ~ 2. The central densities Σ_1 of quiescent galaxies decline slightly (by a factor of $\lesssim 1.7$) from $z \sim 2$ to $z \sim 0$, while for star-forming galaxies Σ_1 increases with time, at fixed mass. We show that the central density Σ_1 has a tighter correlation with specific star-formation rate (sSFR) than Σ_m and for all masses and redshifts galaxies with higher central density are more prone to be quenched. Reaching a high central density ($\Sigma_1 \gtrsim 10^{10}\ M_\odot\ \mathrm{kpc}^2$) seems to be a prerequisite for the cessation of star formation, though a causal link between high Σ_1 and quenching is difficult to prove and their correlation can have a different origin.

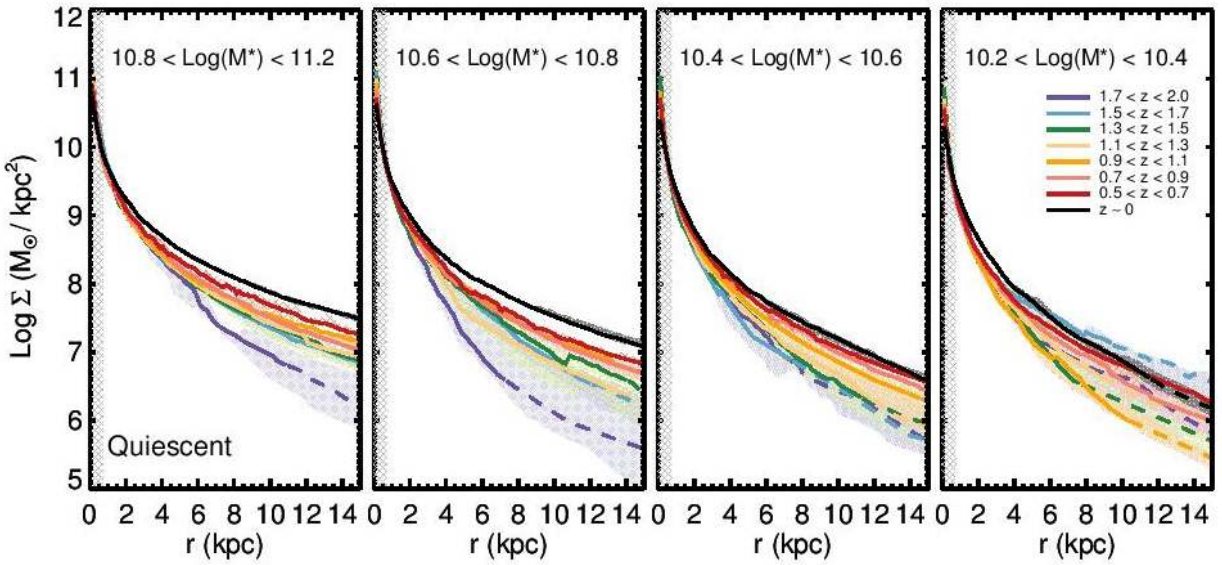

Figure 7. The comparison of the stellar mass density profiles of quiescent galaxies from $z \sim 2$ to $z \sim 0$. Quiescent galaxies are split into four stellar mass bins, decreasing from left to right panel. The shaded regions depict the errors affecting the medians. At all mass bins, the most significant changes of their mass profiles can be seen in the outer regions of these galaxies, i.e., quiescent galaxies at low-z have extended stellar mass profiles comparing to their counterparts at high-z. We caution that the time evolution of individual galaxies cannot easily be seen from this figure, as it compares galaxies at fixed mass bins and individual

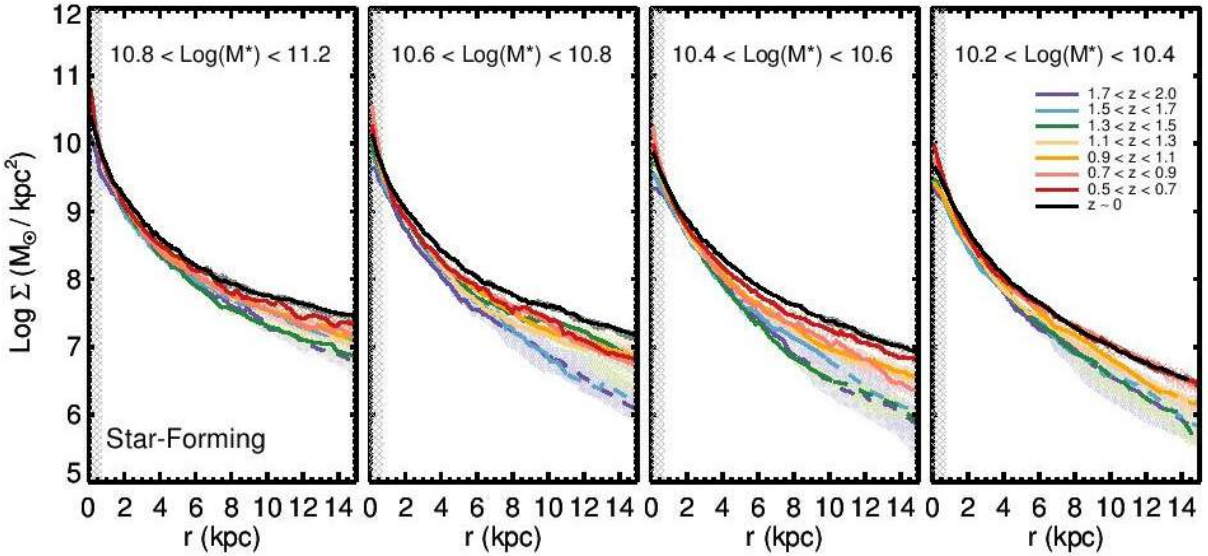

Figure 8. The radial density profiles of star forming galaxies at different epochs (color-lines) and at different mass bins (different panels). The comparison of density profiles at different epochs reveals that star forming galaxies at later times have assembled stellar masses at both inner and outer regions comparing to their high-z counterparts, though the central density varies little with redshift while the density in the outer regions grows substantially. These differences is more prominent for objects within $\log(M_*/M_\odot) = 10.4-10.8$. The massive star forming galaxies ($10.8-11.2 M_\odot$) have little differences (mostly in their outer regions), up to $z \sim 1.5-2$ indicating that stellar mass profiles of these objects grow self-similarly at all epochs.

Сравнение эволюции размеров и плотности галактик без звездообразования и с оным

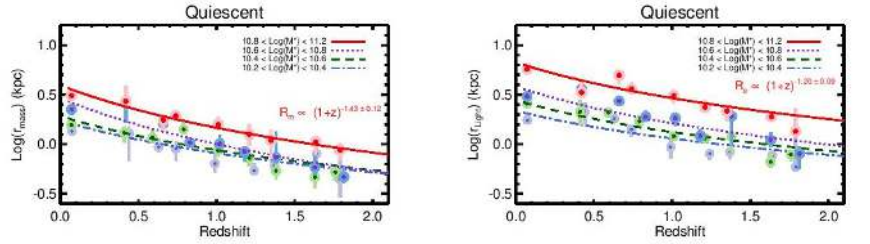

Figure 9. Left Panel: The evolution of half-mass radii from $z \sim 2$ to $z \sim 0$ for quiescent galaxies, for different mass bins. Right Panel: The half-light size evolution for the same galaxies in the left panels. The symbols are the median sizes at each redshift bin and the error bars show the standard errors. The lines and are the best fit to the original data points assuming $(1+z)^a$. The mass-weighted sizes of quiescent galaxies increases by a factor of ~ 4 since $z \sim 2$. The rate of half-mass size evolution is slightly faster than half-light sizes. Similar to Figure 7 & 8, this is not reflecting the size evolution of individual galaxies.

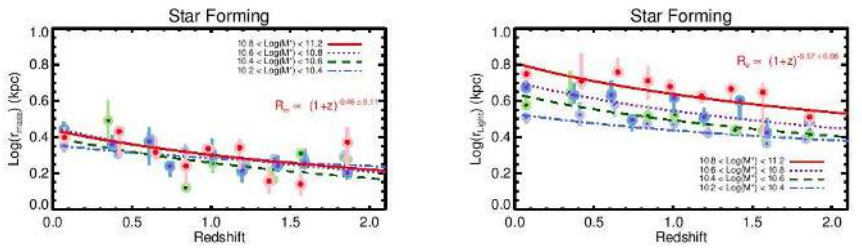

Figure 10. Similar to Figure 9 but for star-forming galaxies. The mass-weighted sizes of star-forming galaxies increase slowly with cosmic time and depend only weakly on stellar mass. This indicates that the central regions and the outskirts have to grow concurrently: the stellar mass profiles have to grow in the central region as well as in the outskirts.

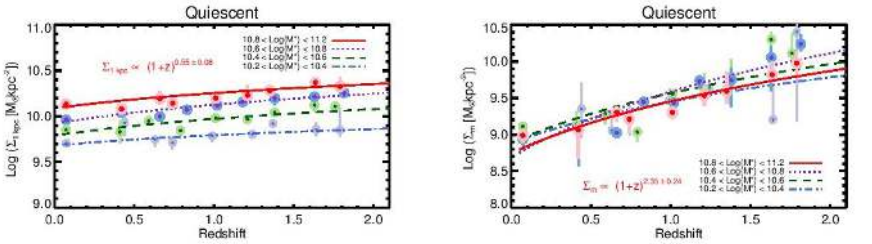

Figure 11. Left Panel: The evolution of central mass density with 1 kpc, Σ_{1kpc} from $z \sim 2$ to $z \sim 0$ for quiescent galaxies, for different stellar mass bins (different colors). The central densities of quiescent galaxies decline slightly with redshift, with the rate of $(1+z)^{0.55\pm0.06}$ for most massive ones. Right Panel: The evolution of surface density at r_m (Σ_m) for quiescent galaxies at different masses with time. The Σ_m declines sharply from $z \sim 2$ to present due to higher surface densities at outer regions of quiescent galaxies in the lower redshifts compare to their analogous at high-z.

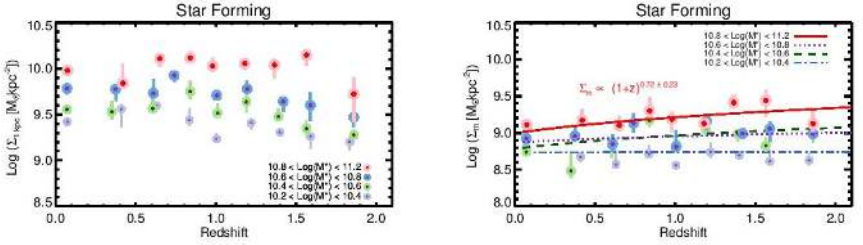

Figure 12. The same as Figure 11, but for star-forming galaxies. The surface density at effective mass radii (Σ_m) declines slightly, specially for the most massive ones, however the changes are very slow for intermediate and low masses. The central densities (Σ_1) increases with time for these galaxies up to $z \sim 0.5$ and remain relatively constant. This shows again the changes of stellar masses in the inner and outer regions. We emphasize that the trends are very mild.

Quenching?! Управляется центральной плотностью?!

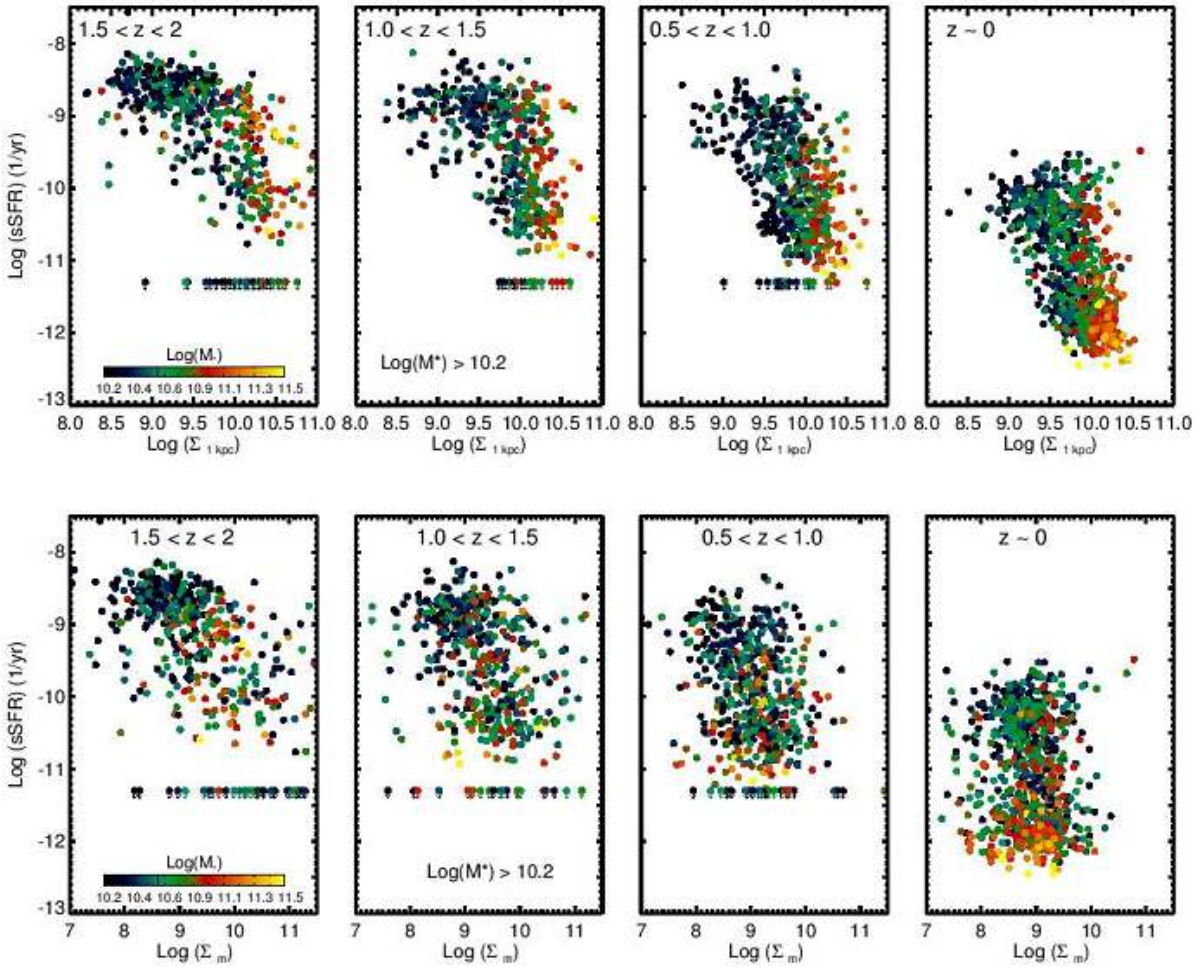

Профили плотности: red, green, blue - сравнение

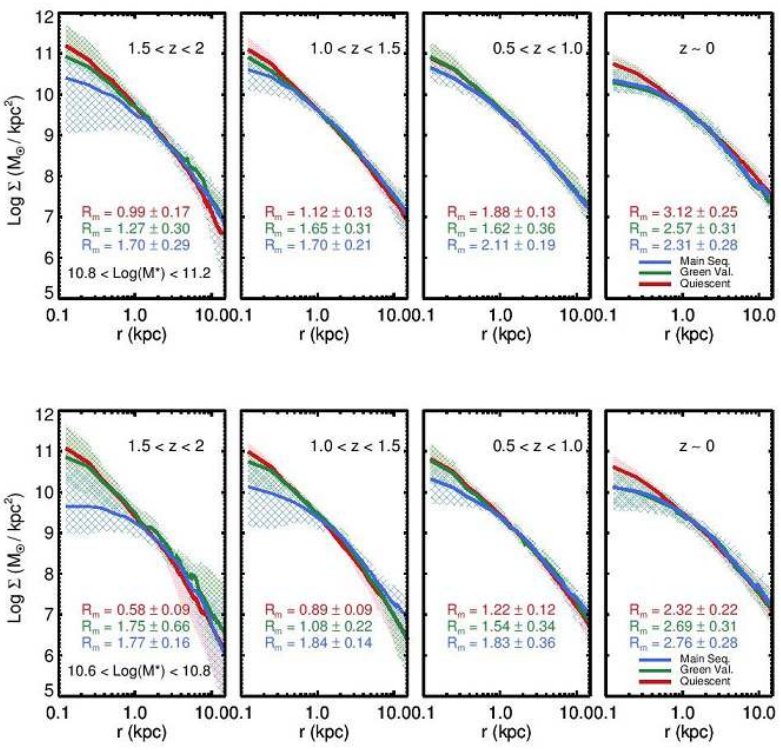

e 16. The stellar mass profiles of galaxies at fixed mass (upper and lower rows) in the regions of main sequence, green valley and quenched defined in : 14 and at different redshift intervals (from left to right). Galaxies in the green valley have comparable central densities to quenched galaxies.

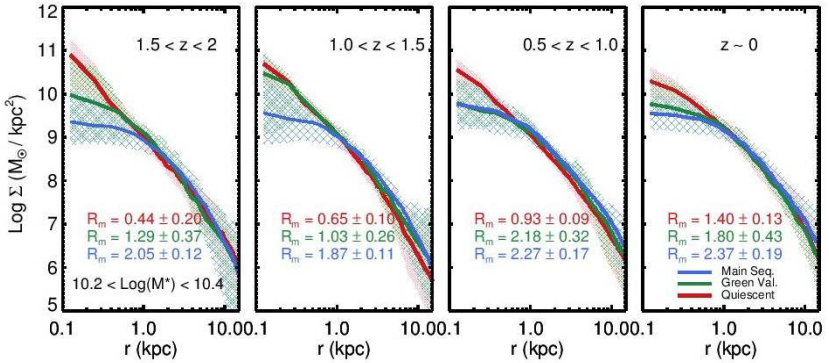

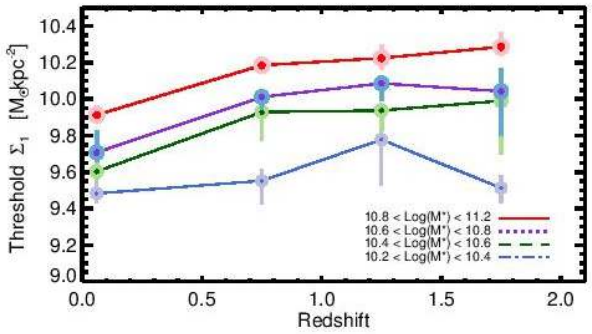

Figure 22. Evolution of Σ_1 threshold values at fixed masses form high-z to low-z, using the median Σ_1 values of galaxies in green valley (gray regions of Figure 15). At fixed mass, the threshold is higher at earlier times.

Критическая центральная плотность

Astro-ph: 1702.02618

THE COS-HALOS SURVEY: METALLICITIES IN THE LOW-REDSHIFT CIRCUMGALACTIC MEDIUM [1]

J. Xavier Prochaska[2], Jessica K. Werk[2,3], Gábor Worseck[4], Todd M. Tripp[5], Jason Tumlinson[6,7], Joseph N. Burchett[5]
Andrew J. Fox[6], Michele Fumagalli[8], Nicolas Lehner[9], Molly S. Peeples[6,7], Nicolas Tejos[10, 11]

[1] Based on observations made with the NASA/ESA Hubble Space Telescope, obtained at the Space Telescope Science Institute, which is operated by the Association of Universities for Research in Astronomy, Inc., under NASA contract NAS 5-26555. These observations are associated with programs 13033 and 11598.

[2] University of California, Santa Cruz; xavier@ucolick.org
[3] University of Washington, Department of Astronomy, Seattle, WA 98195
[4] Max-Planck-Institut für Astronomie, Königstuhl 17, D-69117 Heidelberg, Germany
[5] Department of Astronomy, University of Massachusetts, 710 North Pleasant Street, Amherst, MA 01003-9305
[6] Space Telescope Science Institute, Baltimore, MD, 21218
[7] Department of Physics and Astronomy, Johns Hopkins University, Baltimore, MD, 21218
[8] Institute for Computational Cosmology and Centre for Extragalactic Astronomy, Department of Physics, Durham University, South Road, Durham, DH1 3LE, UK
[9] Center of Astrophysics, Department of Physics, University of Notre Dame, 225 Nieuwland Science Hall, Notre Dame, IN 46556
[10] Millennium Institute of Astrophysics, Santiago, Chile
[11] Instituto de Astrofísica, Pontificia Universidad Católica de Chile, Vicuña Mackenna 4860, Santiago, Chile

ABSTRACT

We analyze new far-ultraviolet spectra of 13 quasars from the $z \sim 0.2$ COS-Halos survey that cover the H I Lyman limit of 14 circumgalactic medium (CGM) systems. These data yield precise estimates or more con-

Профиль плотности HI

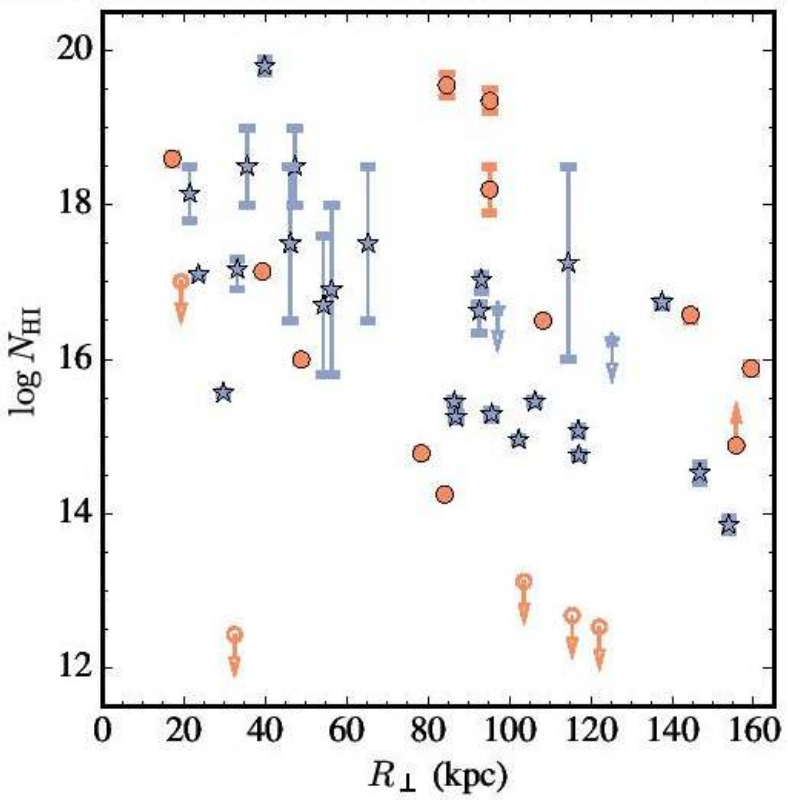

Figure 4. $N_{\rm HI}$ values for the COS-Halos survey versus the projected impact parameter $R_\perp$ to the target galaxy. The measurement of each CGM system is coded by the specific SFR (sSFR) such that red circles indicate a sSFR $< 10^{-11}$ $M_\odot$ yr^{-1}, while blue stars

Металличность

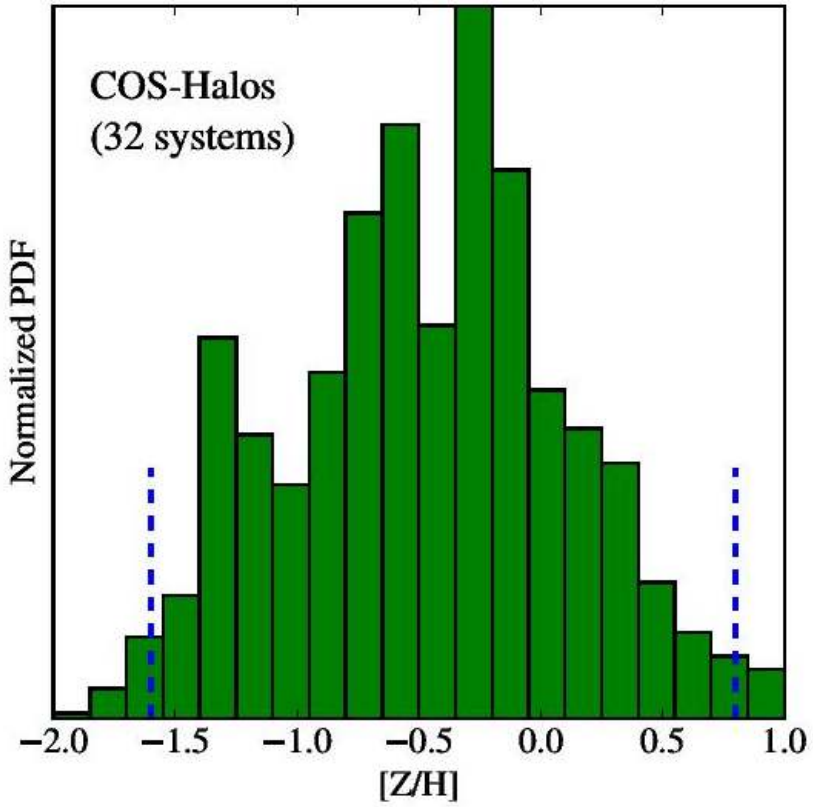

Figure 6. Integrated metallicity PDF for the 32 systems from the COS-Halos dataset with at least one positive detection of a low or intermediate ionic state of a heavy element. This PDF has a median value $[Z/H]_{\rm median} = -0.51$ dex and a 95% c.l. of $[-1.71, 0.76]$, as marked by the blue dashed lines. The data is well-described by a

Всякие корреляции; металличность растет наружу!

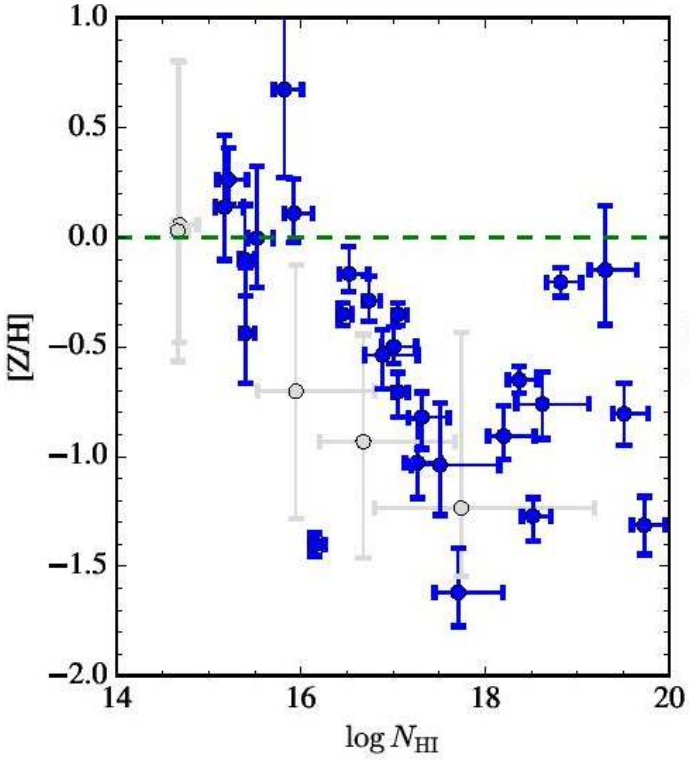

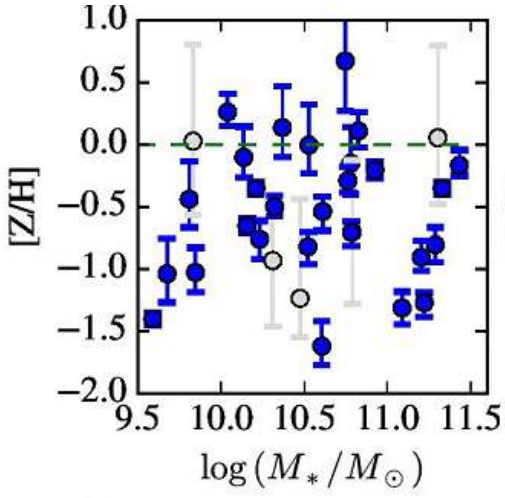

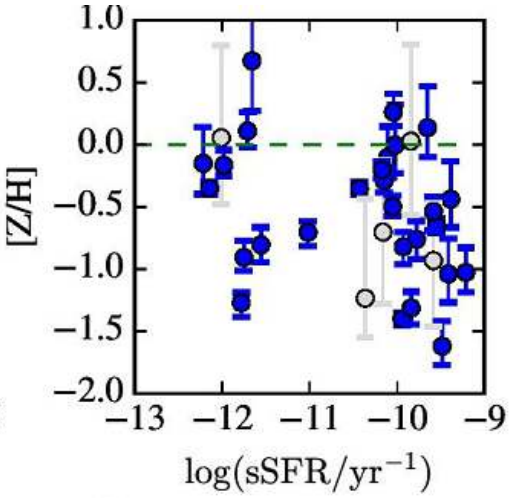

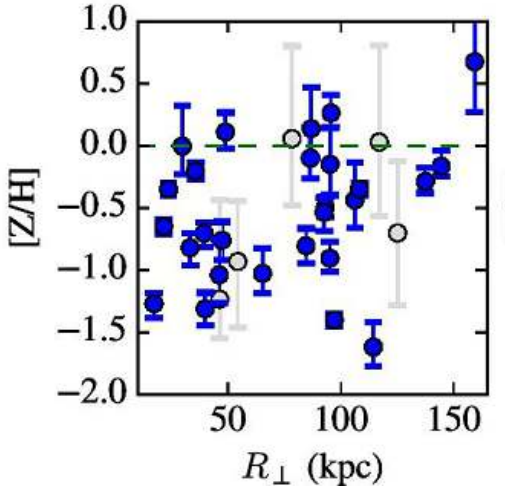

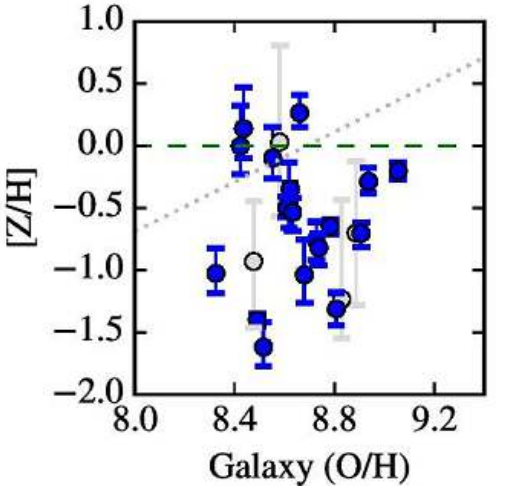

Сравнение с измерениями металличности межгалактического газа в гало разной массы: карлики, нормальные галактики, группы, скопления

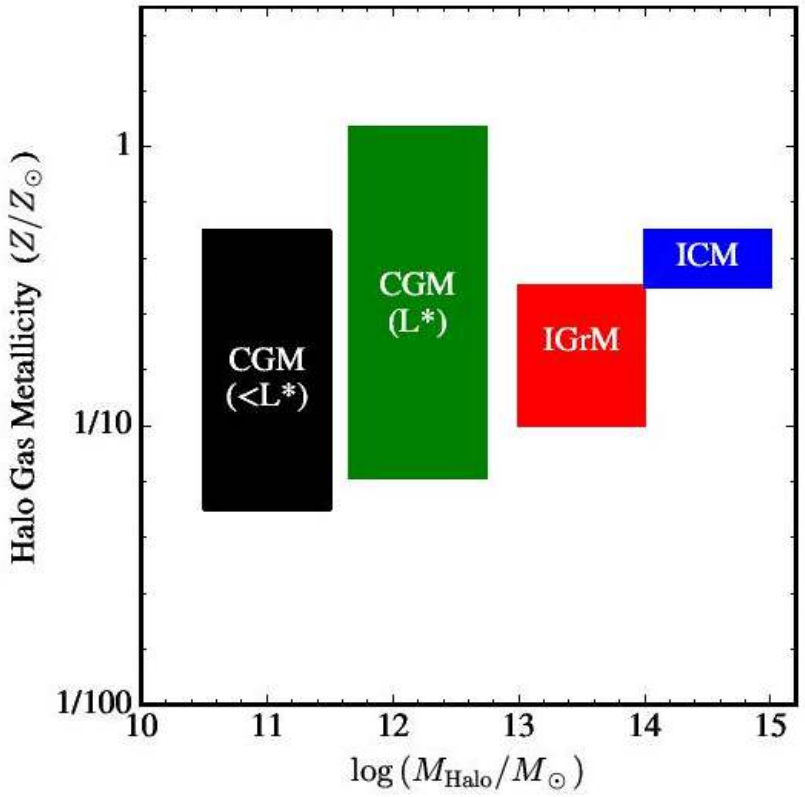

Figure 12. Halo gas metallicity plotted against total halo mass for systems at $z \sim 0$. The measurements were taken from Bordoloi et al. (in prep; sub-L^*), this work (L^*), Rasmussen & Ponman (2009; intragroup medium or IGrM), and Maughan et al. (2008; ICM). There is a general trend toward higher halo metallicity with increasing mass although we stress that the individual galaxies show